IEEE Photonics Journal
An IEEE Photonics Society Publication

Open Access

Wavelength-Tunable Filters Utilizing Arrayed Waveguide Gratings for Colorless/Directionless/Contentionless Optical Signal Drop in ROADMs

Volume 7, Number 1, February 2015

Shoichi Takashina
Yojiro Mori
Hiroshi Hasegawa, Member, IEEE
Ken-Ichi Sato, Fellow, IEEE
Toshio Watanabe, Member, IEEE

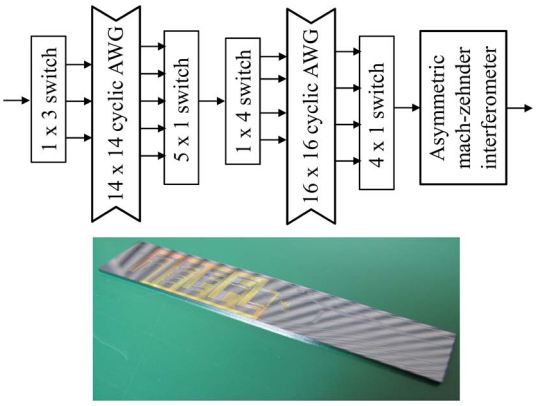

DOI: 10.1109/JPHOT.2015.2400397
1943-0655

Wavelength-Tunable Filters Utilizing Arrayed Waveguide Gratings for Colorless/Directionless/Contentionless Optical Signal Drop in ROADMs

Shoichi Takashina,[1] Yojiro Mori,[1] Hiroshi Hasegawa,[1] *Member, IEEE*, Ken-Ichi Sato,[1] *Fellow, IEEE*, and Toshio Watanabe,[2] *Member, IEEE*

[1]Department of Electrical Engineering and Computer Science, Nagoya University, Nagoya 464-8603, Japan
[2]NTT Device Innovation Center, NTT Corporation, Atsugi 243-0198, Japan

DOI: 10.1109/JPHOT.2015.2400397

Manuscript received January 13, 2015; revised January 30, 2015; accepted February 2, 2015. Date of publication February 4, 2015; date of current version February 19, 2015. This work was supported in part by NICT and KAKENHI under Project 26220905. Corresponding author: S. Takashina (e-mail: s_takasi@echo.nuee.nagoya-u.ac.jp).

Abstract: The wavelength-tunable filter is a key device for creating colorless, directionless, and contentionless reconfigurable optical add–drop multiplexers. Although arrayed-waveguide gratings (AWGs) can realize compact and cost-effective tunable filters, crosstalk in wavelength-division-multiplexing systems increases as the frequency grid spacing decreases. To resolve this problem, we propose a tunable-filter architecture that can eliminate the crosstalk by utilizing two specific (commeasurable) cyclic AWGs in conjunction with multiple switches based on symmetric Mach–Zehnder interferometers and an asymmetric Mach–Zehnder interferometer (AMZI) filter. To verify the technical feasibility of the proposed architecture, we fabricate a monolithic prototype using planar-lightwave-circuit technology. We confirm, for the first time, its excellent performance by measuring insertion loss, polarization-dependent loss, and bit error ratios (BERs). Alternative tunable-filter configurations employing multiple AMZI-based filters are newly investigated for future applications.

Index Terms: Reconfigurable optical add–drop multiplexer (ROADM), tunable filter, arrayed waveguide grating (AWG).

1. Introduction

The present IP traffic is increasing 21% annually, and this trend is expected to continue in the future sustained by the rapidly-growing video traffic and mobile-data traffic [1]. To accommodate the traffic, wavelength-division multiplexing (WDM) has been extensively introduced. Reconfigurable optical add–drop multiplexers (ROADMs) can cost-effectively realize the add/drop and cross-connection of WDM signals. However, current ROADMs are mostly operated in a static manner. Their lack of flexibility prevents us from implementing the dynamic software-defined networks (SDNs) needed in the near future [2], [3]. To resolve this issue, future ROADMs should have the colorless/directionless/contentionless (C/D/C) add–drop capabilities [4]. The colorless add/drop function means that any transponder can transmit/receive any wavelength; the directionless function denotes that any transponder can connect to any outgoing/incoming fiber; the

contentionless function ensures that all the transponders can access fibers and/or wavelengths in a mutually-independent manner. These C/D/C functions enable ROADMs to be operated flexibly and dynamically, which is a key to attaining SDN.

The C/D/C add/drop part can be realized with matrix switches or a combination of splitter-switches and tunable filters [5]–[9]. Unfortunately, matrix-switch-based add/drop architectures will not be suitable for creating future large-port-count ROADMs because the scale (or the difficulty) of matrix switches increases with the power of the number of add/drop channels. On the other hand, the combination of splitter-switches and tunable filters can deal with the ever-increasing traffic since the numbers of splitter ports, switches, and tunable filters linearly increase with the number of supported channels. Splitter-switches can be produced at a low cost; therefore, the tunable filter is the key to achieving total effectiveness.

So far, we have developed compact and cost-effective tunable filters by combining two co-prime cyclic arrayed-waveguide gratings (AWGs) and switches based on symmetric Mach–Zehnder interferometers (SMZIs). The tunable filters, however, suffer from the adjacent-passband problem, that is, the passbands of the two co-prime cyclic AWGs tend to partly overlap which triggers inter-channel crosstalk. The adjacent-passband problem becomes critical as the channel spacing decreases, e.g., the 25-GHz frequency grid.

To overcome this difficulty, we propose a tunable-filter architecture that can completely eliminate the adjacent-passband problem [10]. The proposed architecture employs two commeasurable cyclic AWGs. Although multiple wavelengths are output simultaneously, residual undesired wavelengths are removed by introducing an asymmetric Mach–Zehnder interferometer (AMZI). With this proposal, we can achieve low-crosstalk tunable filters without any additional complexity. To prove its technical feasibility, we fabricate a tunable-filter prototype using the planar-lightwave-circuit (PLC) technology; it can demultiplex 192 wavelengths on the 25-GHz grid. This paper is the first to measure its filtering characteristics in terms of insertion loss, polarization-dependent loss (PDL), and bit-error ratio (BER). The results confirm good filtering performance. In addition, we investigate the effectiveness of other tunable-filter alternatives that exploit multiple AMZIs, which will lead to future applications.

The organization of this paper is as follows: Section 2 reviews our previously proposed tunable-filter configurations [11], [12] based on AWGs and switches and investigates the mechanism of crosstalk generation. In Section 3, we propose a tunable-filter architecture that eliminates the crosstalk problem. Section 4 details the experiments used to validate the effectiveness of the proposed tunable-filter architecture, where a tunable-filter prototype is fabricated with the PLC technology. In Section 5, we discuss the effectiveness achieved by introducing multiple AMZI-based filters into our tunable-filter architecture. Finally, we conclude this paper in Section 6.

2. Conventional Tunable-Filter Architecture Based on AWGs and Switches

2.1. C/D/C ROADM With Tunable Filters

Fig. 1 depicts the schematic of a ROADM that attains C/D/C add/drop capability. The drop part utilizes a combination of splitter-switches and tunable filters. First, incoming multiple wavelength channels are amplified by an erbium-doped-fiber amplifier (EDFA) as necessary (not shown in Fig. 1) and then distributed by an optical-power splitter. After that, a desired incoming fiber is selected by a switch and a target drop channel is extracted by a tunable filter. In this way, each receiver can access an arbitrary channel in an arbitrary input fiber without any restriction. Since the splitter and switch have relatively low cost, the tunable filter is a key device in minimizing the overall ROADM cost, when the number of channels accommodated is large. The requirements for the tunable filter are compactness and low crosstalk. The add part is almost the same as the drop part though tunable filters are not necessary; therefore, its description is omitted below. The tunable filter function can be performed when we apply coherent detection; however, coherent detection will not always be available in particular in very cost-sensitive areas such as metro and metro access area where substantial numbers of 10 Gbps transmission components will be kept in use

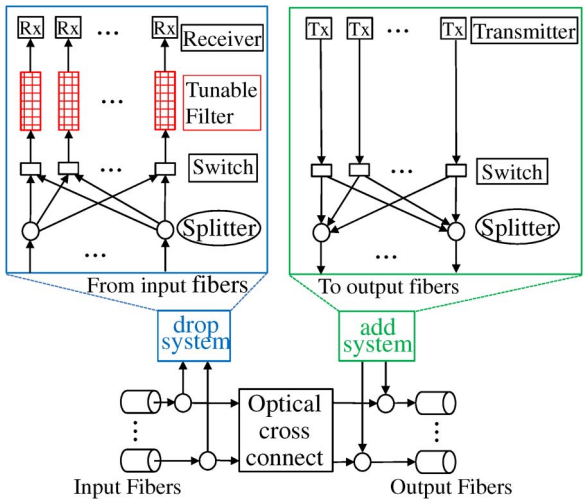

Fig. 1. Schematic of a C/D/C ROADM employing tunable filters.

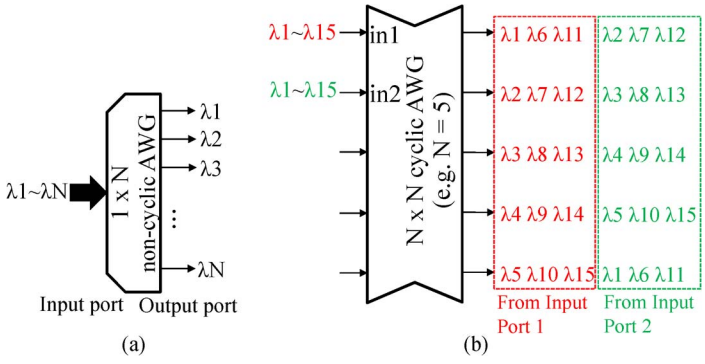

Fig. 2. Basic operation of (a) a non-cyclic AWG and (b) a cyclic AWG.

for a long time. Furthermore, the allowable optical input power to the coherent receiver is limited by the dynamic range of the photodetectors. If the total receiver input power of wavelength channels and amplified-spontaneous-emission (ASE) noise is large, the photodetectors will be damaged. In contrast, when the receiver input power is small, the electrical signal obtained after coherent detection is also small allowing the signal-to-noise ratio (OSNR) to be degraded by the thermal noise of the electrical circuit. The receiver input power should, thus, be properly controlled with an optical tunable filter to maximize the target-channel power input to the photodetectors.

2.2. Operation Principle of AWGs

Fig. 2(a) and (b) shows, respectively, the operation principle of a $1 \times N$ non-cyclic AWG and an $N \times N$ cyclic AWG, where "$P \times Q$" denotes P input ports and Q output ports. In Fig. 2(a), the $1 \times N$ non-cyclic AWG can independently divide up to N wavelengths aligned at fixed intervals in the frequency domain. As shown in Fig. 2(b), the $N \times N$ cyclic AWG can also separate wavelengths, but it has two distinct features: One is that the output port depends on both the input port and the wavelength. The other is that wavelengths are output from the same port every N wavelengths. In other words, its free-spectral range (FSR) is same as the total frequency-slot bandwidth of N wavelengths.

2.3. Tunable Filter Based on a Single Non-Cyclic AWG and SMZI-Based Switch

Fig. 3 shows the basic configuration of a tunable filter that utilizes a single non-cyclic AWG and a single switch (see Fig. 3; 96×1 switch) based on SMZIs. In this architecture, input WDM

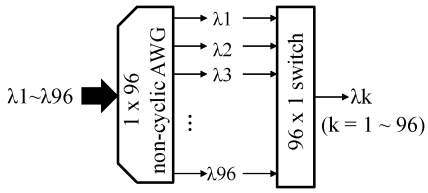

Fig. 3. Tunable filter using a single non-cyclic AWG and SMZI-based switch.

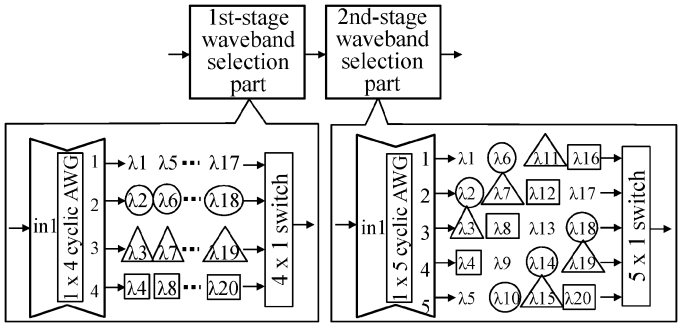

Fig. 4. Two-stage tunable-filter structure using two cyclic AWGs and two SMZI-based switches, where the degrees of the two cyclic AWGs are co-prime.

signals are demultiplexed by the non-cyclic AWG, and one of them is selected by the SMZI-based switch. With this configuration, an arbitrary wavelength can be extracted. However, this architecture is not effective because the switch scale becomes huge as the number of supported channels increases. If the demultiplexing of 96 wavelengths is assumed, a 96$\times$ 1 switch is required. Note that the 96 $\times$ 1 switch would need 95 2 $\times$ 1 SMZIs, which is clearly impractical.

2.4. Tunable Filter Based on a Two-Stage Cyclic AWG and SMZI-Based Switch

To realize switches of practical scale, we have proposed a tunable-filter configuration based on two-stage waveband and wavelength selection as shown in Fig. 4 [11], [12]. Each selection part is comprised of a single cyclic AWG and SMZI-based switch. In the first stage, the waveband-selection part, the cyclic AWG divides input wavelengths into multiple wavelength groups called “wavebands,” and one of them is selected by the following switch. At the second stage, the cyclic AWG separates the wavelength group into individual wavelengths and a switch finally selects one of the outputs of the cyclic AWG. The passbands of the first- and second-stage cyclic AWGs must overlap at the desired wavelength; moreover, the degrees of the two cyclic AWGs must be co-prime [13], otherwise multiple wavelengths are simultaneously output from the tunable filter. To explain the two-stage grouping process more specifically, let us assume a tunable filter for 20 wavelengths. It consists of a 1$\times$ 4 cyclic AWG, a 4 $\times$ 1 switch, a 1 $\times$ 5 cyclic AWG, and a 5 $\times$ 1 switch, where λ7 is the target wavelength. The 1 $\times$ 4 cyclic AWG groups the 20 wavelengths into four wavebands, each with five wavelengths. The 4$\times$ 1 switch then selects output port #3 of the 1 $\times$ 4 cyclic AWG to extract the wavelength group that includes λ7, and the 4 $\times$ 1 switch output is sent to the 1 $\times$ 5 cyclic AWG. The 1 $\times$ 5 cyclic AWG demultiplexes the five wavelengths and the 5 $\times$ 1 switch selects output port #2 to extract λ7. Thanks to the two-stage selection, the switch scale is much smaller compared than the single stage switch in Fig. 3. Although increasing the number of stages can offer greater reduction in switch scale, adding more stages induces larger insertion loss and filter narrowing effects; therefore, the two-stage configuration is reasonable [11].

2.5. Tunable Filters With Switch–AWG–Switch Arrangement

Although the two-stage configuration can attain smaller switch scale, there remains room for further switch-scale reduction without increasing insertion loss. To achieve this, we proposed a

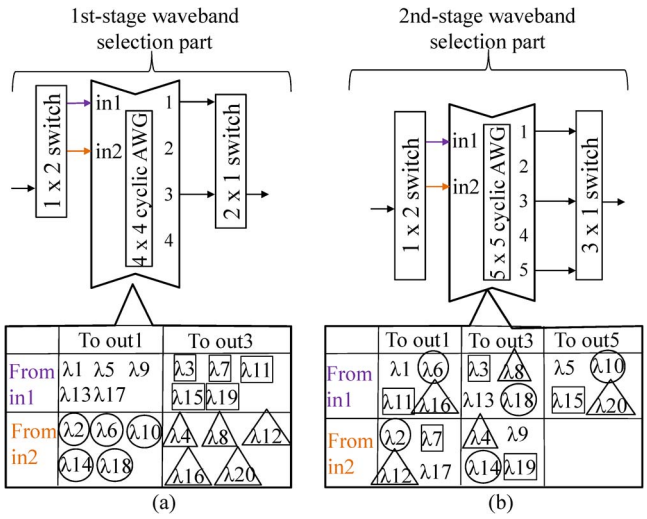

Fig. 5. Two-stage tunable-filter structure using two cyclic AWGs and four SMZI-based switches, where the degrees of the two cyclic AWGs are co-prime.

tunable-filter architecture with switch–AWG–switch arrangement [12]. The arrangement exploits the wavelength routing capability of a cyclic AWG by utilizing both input ports and output ports. Fig. 5 shows the tunable-filter configuration with the switch–AWG–switch arrangement. For simplicity, the number of supported wavelengths is assumed to be 20. The first stage consists of a 1×2 switch, a 4×4 cyclic AWG, and a 2×1 switch in this order; the AWG divides the 20 wavelengths into four groups. Then, one of the four groups is selected and delivered to the second stage consisting of a 1×2 switch, a 5×5 cyclic AWG, and a 3×1 switch. In the same manner, the target wavelength is finally extracted. Using the example shown in Fig. 5, we explain the filtering process when $\lambda 12$ is the target wavelength. The 1×2 switch and the 2×1 switch select input port #2 and output port #3 of the 4×4 cyclic AWG, respectively. In this case, $\lambda 4$, $\lambda 8$, $\lambda 12$, $\lambda 16$, and $\lambda 20$ are output. After that, the 1×2 switch and the 3×1 switch respectively select input port #2 and output port #1 of the 5×5 cyclic AWG. In this case, only $\lambda 12$ can pass through both stages. Thus the target wavelength is extracted by selecting the proper input port and output port of the AWG at each stage.

2.6. Adjacent-Passband Problem

As detailed above, our tunable filters can support a large number of wavelengths with smaller switch scale. However, we found that crosstalk becomes a problem as the frequency grid spacing narrows. In order to resolve this problem, we first identify the cause of the crosstalk. Fig. 6(a) and (b) shows examples of passbands of the used two co-prime cyclic AWGs, where ideally-expected passbands and actual passbands are considered, respectively. If the cyclic AWGs have rectangular passbands aligned accurately on the prescribed frequency grid (e.g. the ITU-T grid), crosstalk does not occur. However, passbands of cyclic AWGs generally follow a Gaussian function and their center frequencies can deviate from the grid [14]. Given this condition, passbands of the first- and second-stage cyclic AWGs can partially overlap at undesired frequencies and hence crosstalk remains after the tunable filter. This crosstalk mostly occurs when the passbands of the two cyclic AWGs are next to each other; therefore, we call this the "adjacent-passband problem."

3. Proposed Tunable-Filter Architecture That Eliminates Crosstalk

To eliminate the crosstalk that stems from the adjacent-passband problem, we propose a tunable-filter architecture that consists of two waveband wavelength selection parts and a

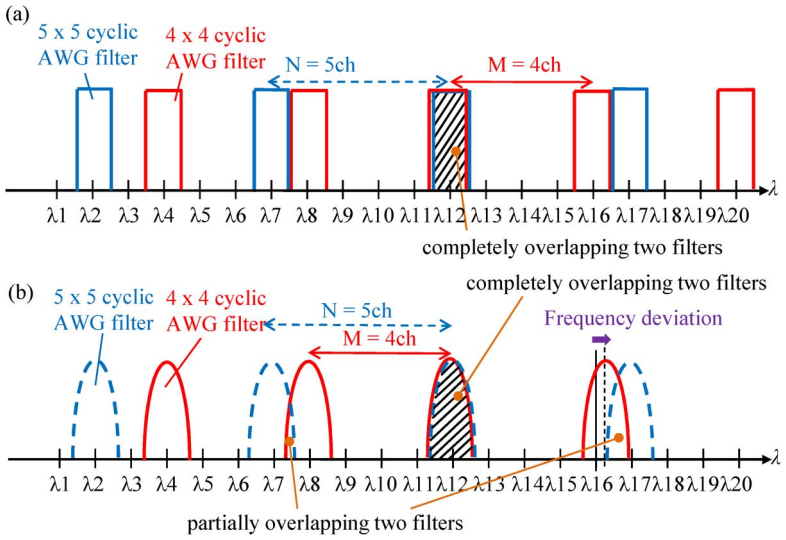

Fig. 6. Passbands of two cyclic AWGs whose degrees are co-prime each other, (a) the ideal case where the cyclic AWGs have the rectangular passbands and have no passband-frequency deviation, and (b) the actual case where the cyclic AWGs have the Gaussian-shaped passbands with passband-frequency deviation.

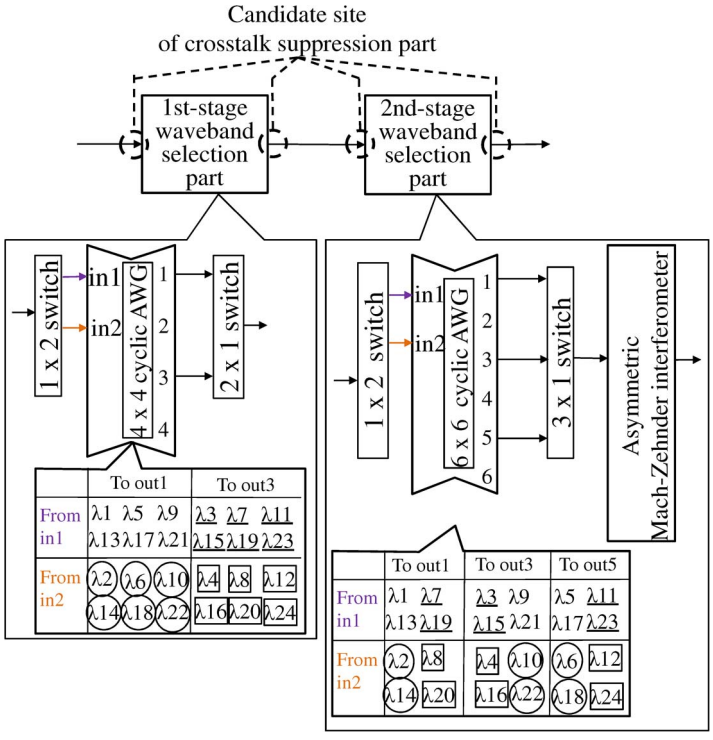

Fig. 7. Proposed two-stage tunable-filter structure using two cyclic AWGs, four SMZI-based switches, and an AMZI-based filter, where the degrees of the two cyclic AWGs must be commeasurable.

crosstalk-suppression part using an AMZI, as shown in Fig. 7. Note that the degrees of the cyclic AWGs in the two waveband-selection parts must have a common factor, while those of the previous schemes shown in Figs. 4 and 5 must be co-prime. For explanation simplicity, our example assumes the demultiplexing of 24 wavelengths. In the first-stage waveband-selection

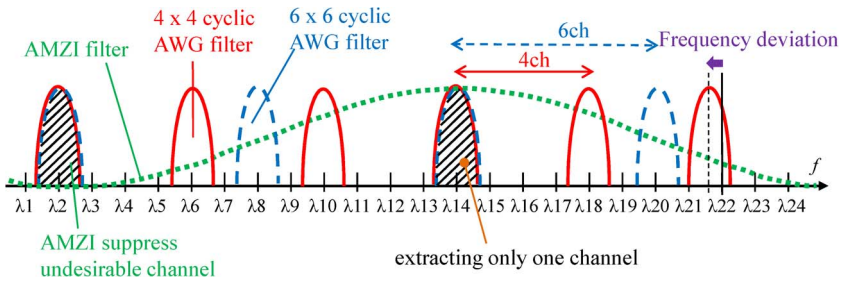

Fig. 8. Passbands of two cyclic AWGs and an AMZI-based filter, where degrees of two cyclic AWGs are commeasurable.

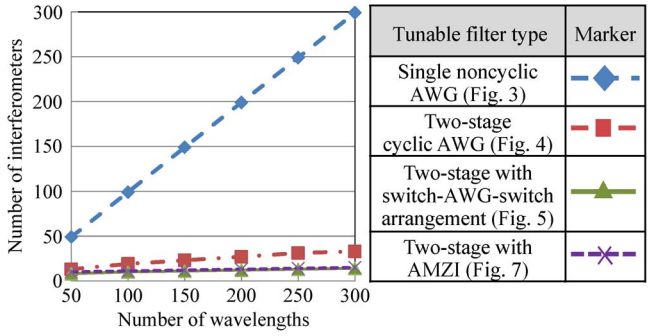

Fig. 9. Necessary number of interferometers as a function of the number of supported wavelengths.

part, a 4 × 4 cyclic AWG divides the 24 wavelengths into four groups according to the input port and output port selected; six wavelengths in the same group are depicted by the same markers in Fig. 7. One of the four groups is selected by the combination of a 1 × 2 switch AWG, and a 2 × 1 switch and is delivered to the second-stage wavelength-selection part. The second stage consists of a 1× 2 switch, a 6 × 6 cyclic AWG, and a 3 × 1 switch. The group selected in the first stage is further divided in the same manner. However, multiple wavelengths, shown by the same markers, are output from the same output port of the 6 × 6 cyclic AWG. If $\lambda 14$ is the target wavelength, $\lambda 2$ is also output from the same port as shown in Fig. 8. To extract only $\lambda 14$, we introduce an AMZI that has a broader passband frequency filter at the final stage. Thus, the target wavelength is extracted. Note that the two commeasurable cyclic AWGs never have passbands next to each other, hence the adjacent-passband problem is completely avoided even if passband-frequency deviation exists. It is difficult to make the FSR of the AMZI narrow, since the crosstalk becomes large as the frequency-grid spacing decreases. Accordingly, the combination of the AMZI and the cyclic AWGs is needed to suppress the crosstalk.

Since the AMZI has a similar structure to the SMZI, it can be easily implemented. Fig. 9 shows the relationship between the number of supported wavelengths and that of 2 × 1 MZ interferometer elements, where we assume that an $L \times 1$ (or a $1 \times L$) switch consists of $L - 1$ 2 × 1 interferometer elements. When demultiplexing 100 wavelengths, the two-stage tunable filter with switch–AWG–switch arrangement reduces switch scale by 94% compared to the single-stage non-cyclic configuration or by 50% compared to the two-stage configuration without switch–AWG–switch arrangement. This substantial switch-scale reduction enables compact implementation. Moreover, even when the AMZI is introduced to the switch–AWG–switch-arranged two-stage tunable filter, the number of necessary interferometers is almost the same as that for the tunable filter without any AMZI; it is generally larger by 1. The proposed tunable-filter configuration hardly increases implementation complexity. Moreover, since the insertion loss of the proposed tunable filter is dominated by that of the cyclic AWGs, introducing the AMZI basically does not increase the total device loss.

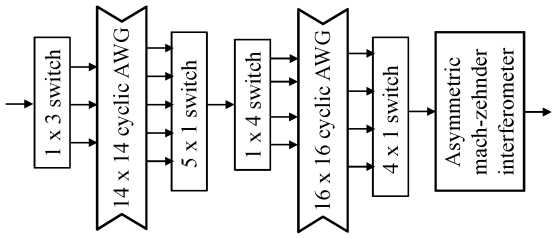

Fig. 10. Configuration of a fabricated tunable-filter prototype.

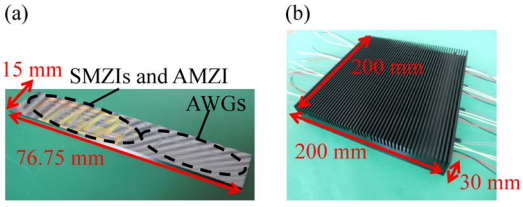

Fig. 11. (a) Tunable filter monolithically fabricated on a PLC chip and (b) module box holding eight PLC chips.

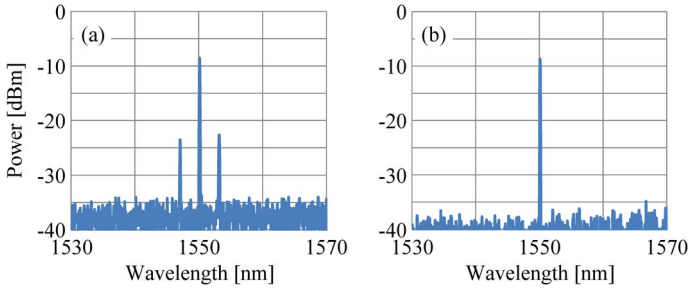

Fig. 12. Measured passbands of (a) the previous tunable filter without AMZI and (b) the proposed tunable filter with AMZI.

4. Experiments

To confirm the technical feasibility of the proposed tunable-filter architecture, we fabricated a prototype monolithically using PLC technology. We expect to use Si photonics technologies in the future, so device size would be further reduced. The prototype was designed to demultiplex 192 channels with 25-GHz spacing ($191.15 + 0.025 \times n$ [THz]; $n = 0 \sim 191$) on the ITU-T grid. The tunable filter consists of a $1\times$ 3 switch, a 14×14 cyclic AWG, a 5×1 switch, a 1×4 switch, a 16×16 cyclic AWG, a 4×1 switch, and an AMZI aligned in this order (see Fig. 10). The power transmittance of the AMZI is the square of a sine function; its FSR and full width at half maximum are 5600 GHz and 2800 GHz, respectively. The fabricated tunable filter chip size was 15×76.75 mm^2 [Fig. 11(a)], which is almost the same as that of our previously developed tunable filter without any AMZI [12]. Moreover, eight tunable filters are implemented in a module box of $200 \times 200 \times 30$ mm^3 [see Fig. 11(b)]. We measured filter performance of the tunable filters without and with an AMZI; the target wavelength was 1550.116 nm (see Fig. 12). The extinction ratio of the proposed tunable filter is improved to 26 dB, a 12 dB improvement from the 14 dB of the previous tunable filter which uses no AMZI. Thus, introducing the AMZI can well suppress the crosstalk caused by the adjacent-passband problem. We observe that the crosstalk caused by the adjacent-passband problem is completely suppressed. We also measured insertion loss and PDL on the ITU-T grid (see Fig. 13). The average and worst insertion losses were, respectively, 9 dB and 11.6 dB; the proposed architecture offers virtually the same insertion loss as

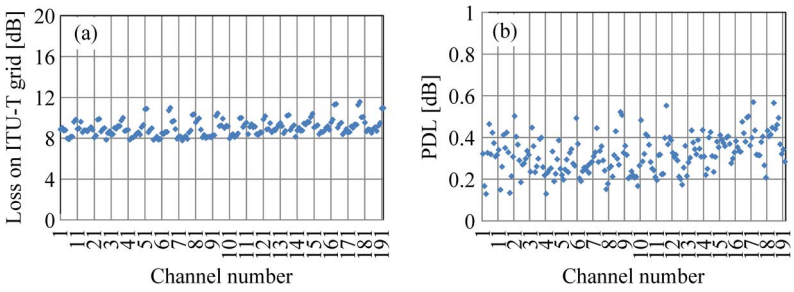

Fig. 13. Transmission characteristics on the 25-GHz ITU-T grid. (a) Insertion loss and (b) PDL.

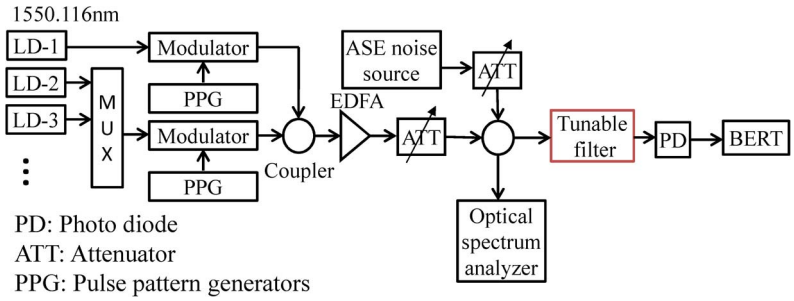

Fig. 14. Experimental setup.

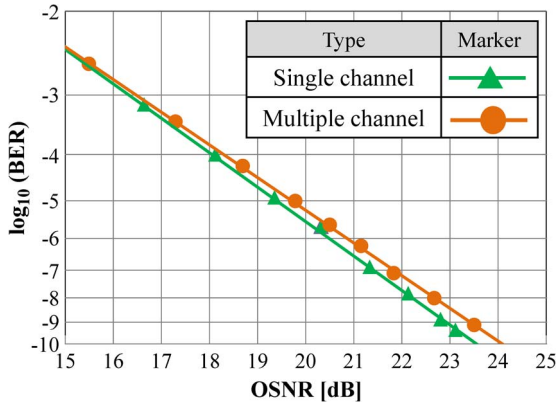

Fig. 15. BER vs. OSNR measured with the tunable-filter prototype.

the previous one. The average and worst PDLs were negligible: 0.3 dB and 0.6 dB, respectively. We also measured the BER characteristics by using the experimental setup shown in Fig 14. Laser diodes (LD) produced multiple wavelengths; one was the target signal, and the others were used as crosstalk sources. Their intensities were modulated at 10 Gbps. After the signals and ASE noise were combined by a coupler, we measured OSNRs with an optical spectrum analyzer. Finally, the signals with ASE noise were launched into the tunable filter to extract the target wavelength, and a BER tester (BERT) measured BERs. Fig. 15 shows the results. The OSNR penalty is 0.6 dB at the BER of 10^{-9}, which is acceptable for practical use.

5. Discussion of Advanced Versions

Advanced versions of the tunable filter described above may utilize multiple AMZIs. As shown in Fig. 16, the $n \times 1$ switch with large port count is generally made by cascading $n-1$ 2×1 SMZI

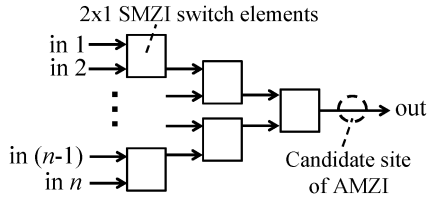

Fig. 16. Structure of a large-port-count switch and optimum location of an AMZI.

TABLE 1

Relation among the maximum common factor of degrees of two cyclic AWGs, the number of AMZIs, and FSRs of AMZIs

The number of AMZIs	Maximum common factor (C)	FSRs of AMZIs
1	2	$2P/C$
2	4	$2P/C$, $4P/C$
3	8	$2P/C$, $4P/C$, $8P/C$
4	16	$2P/C$, $4P/C$, $8P/C$, $16P/C$

elements in a tree structure [15]. To minimize the number of additional AMZIs, it is desirable to place the AMZI at the root of the tree. Therefore, we assume that the maximum number of AMZIs is four since the number of roots is four as shown in Fig. 7. Suppose that the tunable filter uses $M \times M$ and $N \times N$ cyclic AWGs and C is the greatest common factor between M and N. Table 1 summarizes relationship among the number of utilized AMZIs, the common factor C, and the FSRs of AMZIs, where Δf is the frequency spacing between neighboring wavelengths and $P = M \times N \times \Delta f$. As can be seen from Table 1, the use of multiple AMZIs allows larger common factors, which provides more combinations with different degrees of two cyclic AWGs. For example, a 54-wavelength tunable filter should consist of an 8×8 cyclic AWG and a 10×10 cyclic AWG when the maximum common factor C is 2. On the other hand, using $C = 3$ allows the use of a 6×6 cyclic AWG and a 9×9 cyclic AWG, which reduces the AWG footprint. In this way, the use of multiple AMZIs can offer more flexibility in optimizing the design of the tunable filters. Furthermore, since an AMZI can independently divide two wavelengths, introducing an additional AMZI can double the number of available wavelengths without increasing the cyclic-AWG scale. Such a configuration will be useful when the number of utilized wavelength channels increases, e.g., the used frequency band is extended from the C-band to the C+L band.

6. Conclusion

We have proposed and developed compact and low-crosstalk wavelength-tunable filters that will play an important role in creating C/D/C ROADMs that enable the flexible and dynamic operation of networks. Detailed analysis of the filter operation led us to utilize AMZIs to suppress crosstalk. To confirm the feasibility of the tunable filter, we implemented a prototype on a 15×76.75 mm^2 PLC chip. We also verified the good performance of the prototype by measuring passband spectra, insertion loss, PDL, and BER characteristics. Finally, we discussed future expansion of the channel numbers that can be effectively attained with the use of additional AMZIs.

Acknowledgment

The authors are grateful to Dr. M. Okuno and Mr. Y. Jinnouchi of NTT Electronics Co. for their useful discussions.

References

[1] *Cisco Visual Networking Index: Forecast and Methodology*, Cisco, San Jose, CA, USA, 2014.

[2] N. Cvijetic *et al.*, "SDN and OpenFlow for dynamic flex-grid optical access and aggregation networks," *J. Lightw. Technol.*, vol. 32, no. 4, pp. 864–870, Feb. 2014.
[3] M. Channegowda, R. Nejabati, and D. Simeonidou, "Software-defined optical networks technology and infrastructure: Enabling software-defined optical network operations [invited]," *J. Opt. Commun. Netw.*, vol. 5, no. 10, pp. A274–A282, Oct. 2013.
[4] S. Gringeri, B. Basch, V. Shukla, R. Egorov, and T. J. Xia, "Flexible architectures for optical transport nodes and networks," *IEEE Commun. Mag.*, vol. 48, no. 7, pp. 40–50, Jul. 2010.
[5] R. Jensen, A. Lord, and N. Parsons, "Colourless, directionless, contentionless ROADM architecture using low-loss optical matrix switches," presented at the 36th Eur. Conf. Exh. Opt. Commun., Torino, Italy, 2010, Paper Mo.2.D.2.
[6] R. A. Jensen, "Optical switch architectures for emerging colorless/directionless/contentionless ROADM networks," presented at the Opt. Fiber Commun. Conf., Los Angeles, CA, USA, 2011, Paper OThR3.
[7] T. Watanabe *et al.*, "Compact PLC-based transponder aggregator for colorless and directionless ROADM," presented at the Opt. Fiber Commun. Conf., Los Angeles, CA, USA, 2011, Paper OTuD3.
[8] B. Collings, "The next generation of ROADM devices for evolving network applications," in *Proc. Market Focus ECOC*, 2011, pp. 1–19.
[9] W. I. Way, "Optimum architecture for M N multicast switch-based colorless, directionless, contentionless, and flexible-grid ROADM," presented at the Opt. Fiber Commun. Conf. Exposition/Nat. Fiber Optic Eng. Conf., Los Angeles, CA, USA, 2012, Paper NW3F.5.
[10] S. Takashina, Y. Mori, H. Hasegawa, K. Sato, and T. Watanabe, "Low crosstalk wavelength tunable filter that utilizes symmetric and asymmetric Mach–Zehnder interferometers," presented at the Opt. Fiber Commun. Conf., San Francisco, CA, USA, 2014, Paper Th3F.6.
[11] T. Niwa *et al.*, "Novel wavelength tunable filter offering multi-stage selection for colorless, directionless, and contentionless ROADMs," *IEICE Electron. Exp.*, vol. 9, no. 16, pp. 1297–1303, 2012.
[12] T. Niwa, H. Hasegawa, K. Sato, T. Watanabe, and S. Soma, "Compact integrated tunable filter utilizing AWG routing function and small switches," presented at the Opt. Fiber Commun. Conf., Anaheim, CA, USA, 2013, Paper OW1C.2.
[13] T. Niwa, H. Hasegawa, K. Sato, T. Watanabe, and H. Takahashi, "A novel large-scale wavelength routing switch configuration exploiting small arrayed waveguide gratings," presented at the Proc. Asia Commun. Photon. Conf., Guangzhou, China, 2012, Paper ATh2C.4.
[14] Y. Chu, X. Zheng, H. Zhang, X. Liu, and Y. Guo, "The impact of phase errors on arrayed waveguide gratings," *IEEE J. Sel. Topics Quantum Electron.*, vol. 8, no. 6, pp. 1122–1129, Nov./Dec. 2002.
[15] T. S. El-Bawab, *Optical Switching*. New York, NY, USA: Springer-Verlag, 2006, pp. 282–285.